Polymer 49 (2008) 2709–2716

Contents lists available at ScienceDirect

Polymer

journal homepage: www.elsevier.com/locate/polymer

Structure and dynamics of a vinylidene fluoride oligomer and its cyclodextrin inclusion compounds as studied by solid-state ^{19}F MAS and $^{1}H \rightarrow {}^{19}F$ CP/MAS NMR spectroscopy

Hiroto Tatsuno, Yu Koseki, Shinji Ando*

Department of Organic and Polymeric Materials, Tokyo Institute of Technology, Ookayama, Meguro-ku, Tokyo 152-8552, Japan

ARTICLE INFO

Article history:
Received 26 September 2007
Received in revised form 17 March 2008
Accepted 8 April 2008
Available online 11 April 2008

Keywords:
Solid-state NMR
Vinylidene fluoride
Cyclodextrin

ABSTRACT

The molecular structure and dynamics of a vinylidene fluoride oligomer telomerized by carbon tetrachloride (Cl-OVDF) and its inclusion compound (IC) with β-cyclodextrin (β-CD) have been investigated using solid-state ^{19}F magic angle spinning (MAS) and $^{1}H \rightarrow {}^{19}F$ cross-polarization (CP)/MAS NMR spectroscopy. The preferential IC formation of the lower-molecular-weight components with β-CD was used to refine as-received Cl-OVDF. The refined Cl-OVDF with larger molecular weight readily takes γ-form ($tttg^{+}tttg^{-}$) conformation, and it also forms ICs with β-CD (Cl-OVDF/β-CD IC) under a certain condition. ^{19}F MAS NMR indicates that Cl-OVDF chains virtually isolated in the β-CD cavities take no specific conformations even at −40 °C. The temperature dependence of the magnetic relaxation times (T_1^F, $T_{1\rho}^F$) indicates that the Cl-OVDF chains in ICs undergo molecular motions similar to the amorphous phase in the bulk, although the intramolecular spin diffusion among ^{19}F nuclei is more significant in the former because of the one-dimensional confinement.

1. Introduction

Poly(vinylidene fluoride) (PVDF) is a semicrystalline fluoropolymer which takes several polymorphs such as α- ($tg^{+}tg^{-}$ conformation),β- (all-*trans*), and γ-form ($tttg^{+}tttg^{-}$). In particular, β- and γ-form has attracted more attention than α-form because they exhibit significant piezoelectricity due to the intramolecular polarization [1–10]. The α-form crystal predominantly develops from the melt because of the fastest crystallization rate among the three forms. The β-form can be readily obtained by uniaxial drawing of bulks or film taking α-form on heating, while the γ-form can be acquired by annealing of α-form near the melting temperature [1–3,5,10]. In contrast to PVDF, the conformations of vinylidene fluoride oligomers (OVDF) are strongly affected by molecular weight (*i.e.* degree of polymerization) or terminal groups rather than by thermal conditions for crystallization. Tashiro and Hanesaka [4] have extracted monodisperse oligomers ($CF(CF_3)_2$–$(CH_2CF_2)_n$–I, where $n = 6$–12) from polydisperse OVDF by supercritical fluid chromatography. Using X-ray diffractions of single crystals and infrared spectroscopy (IR), they demonstrated that the shorter oligomers ($n = 6$–10) are likely to take α-form, while the longer ($n = 11$–12) predominantly take γ-form. Meanwhile, other researchers have reported that the OVDF telomerized by carbon tetrachloride (CCl_3–$(CH_2$–$CF_2)_n$–Cl) and crystallized from the melt can take various conformations according to their molecular lengths: β (for $n < 10$), α ($n = 10$–16), and γ ($n > 16$) forms [11–13]. Such difference in conformation is responsible for the bulk properties: polarized β- and γ-crystallite of OVDF also exhibits ferroelectricity like PVDF [14,15]. However, special techniques are required not only for controlling the chain lengths but also for extracting a component with a certain chain length. If chain lengths and conformations of OVDF can be precisely controlled or readily altered, it will be of great significance for polymer industries.

As one of the facile methods, we focused on the use of cyclodextrin (CD) inclusion compounds (ICs). CD is a family of cyclic oligosaccharides composed of several D-glucopyranose units. The CDs containing six, seven, and eight glucopyranose units are known as α-, β-, and γ-CD, respectively. They show versatile demands for various scientific fields because of their capability to include polymers as well as small molecules in their hydrophobic cavities [16–19]. It is well known that CDs are likely to form channel-type ICs with polymers such as poly(ethylene glycol), poly(propylene glycol), and poly(methyl vinyl ether) [20–22]. Moreover, the conformations and dynamics of polymers incorporated in CD channels are often different from those in bulk [23–27]. For instance, polymer chains of poly(oxyethylene) (POE) take *ttg* conformation (consisting of *trans*-like C–C–O–C and *gauche*-like O–C–C–O) in bulk. In contrast, POE chains confined in α-CD cavity mainly take

* Corresponding author. Tel.: +81 3 5734 2137; fax: +81 3 5734 2889.
E-mail address: sando@polymer.titech.ac.jp (S. Ando).

0032-3861/$ – see front matter © 2008 Elsevier Ltd. All rights reserved.
doi:10.1016/j.polymer.2008.04.010

all-*trans* conformation, in which '*gauche* defects' can travel along the chains [23]. One of the most influential factors for the formation of solid-state ICs is whether a guest molecule fits in a CD cavity or not [20–22]. Fluorinated linear oligomers are more likely to form IC with β-CD, which is in contrast to the fact that non-fluorinated oligomers and polymers most efficiently form ICs with α-CD [28–31].

Solid-state ^{19}F magic angle spinning (MAS) NMR is a powerful tool to investigate the structure and dynamics of fluorinated polymers for the following reasons. First, ^{19}F is one of the most sensitive nuclei due to the 100% of natural abundance and the high magnetogyric ratio (94% of ^{1}H nuclei). Second, the wide chemical shift range of ^{19}F nuclei allows us the more detailed analysis of the chemical structures, conformations, and molecular mobility than conventional $^{1}H \rightarrow {}^{13}C$ cross-polarization (CP)/MAS NMR. Furthermore, $^{1}H \rightarrow {}^{19}F$ CP/MAS NMR has a potential advantage for the analysis of phase structures and molecular dynamics of the materials containing both fluorine and hydrogen atoms in their systems [32–40]. Solid-state NMR spectroscopy is also used for CD ICs to analyze molecular dynamics of both host and guest molecules [23–28]. We have previously reported the structure and dynamics of CD ICs consisting of perfluoroalkane (PFA) and β-CD using solid-state ^{19}F MAS NMR and $^{1}H \rightarrow {}^{19}F$ CP/MAS NMR [28]. We showed that PFA molecules successfully form channel-type ICs with β-CD and the PFAs in the channel undergo more rapid internal rotation of the end group than neat PFAs. In addition, a part of PFA molecules comes out of the β-CD channel as the temperature increases.

In this study, we performed ^{19}F MAS and $^{1}H \rightarrow {}^{19}F$ CP/MAS NMR measurements to investigate the molecular structure and dynamics of chlorine-terminated OVDF (Cl-OVDF) with the aid of solution ^{19}F NMR, FT-IR spectroscopy, and differential scanning calorimetry (DSC). Moreover, ICs of Cl-OVDF/β-CD were prepared for investigating the conformations and dynamics of Cl-OVDF chains in the ICs with those in the bulk.

2. Experimental section

2.1. Materials

Polydisperse Cl-OVDF was kindly supplied from Kureha Corporation. According to the literature [11,12], the number-average degree of polymerization of the sample was estimated as ca. 9. The as-received OVDF was waxy and sticky probably due to considerable amount of lower-molecular-weight (LW) components and impurities. In fact, the as-received sample may contain di-*n*-propyl peroxydicarbonate ($(C_3H_7OCOO)_2$) used as a catalyst in the telomerization processes [11]. β-CD was purchased from Wako Pure Chemical Industries, Ltd. and recrystallized from distilled water. Cl-OVDF/β-CD ICs were prepared as follows. First, Cl-OVDF (0.40 g) was dissolved in a (1:1) solvent mixture of acetone and tetrahydrofuran (THF) and heated to 60 °C. On the other hand, β-CD aqueous solution (100 ml) was heated at 60 °C and then added to the Cl-OVDF solution by portions with vigorous stirring. After the intermixture was slowly cooled to room temperature with stirring, the solution became slurry, and then yielded a white precipitate after 72 h. The resultant precipitate was filtered and washed with the solvent mixture and water alternately to remove uncomplexed Cl-OVDF and β-CD, respectively. After washing for three times, the product was dried under vacuum at ambient temperature to remove the solvents.

2.2. Nuclear magnetic resonance

Solid-state ^{19}F NMR experiments were performed on a JEOL EX spectrometer operating at resonance frequencies of 282.65 MHz for fluorine and 300.40 MHz for proton with a Chemagnetics APEX $^{19}F/^{1}H$ dual-tune probe and 4 mm o.d. zirconia Pencil rotors. Samples were spun at the magic angle at a rate of $\omega_r = 15$ kHz. The magic angle was adjusted by monitoring the ^{19}F signal of α,α,α-trifluorotoluene included in *p*-*tert*-butylcalix[4]arene [41]. Temperature inside the rotor was calibrated using ^{1}H chemical shifts of ethylene glycol adsorbed on tetrakis(trimethylsilyl)silane spun at the same rate (15 kHz) [42]. The temperatures were precisely controlled between −40 and 100 °C. Fluorine chemical shifts are referenced to hexafluorobenzene, which is assigned a value of −163.6 ppm with respect to trichlorofluoromethane ($CFCl_3$) with 85 kHz of proton decoupling field to correct the Bloch–Siegert effect [40]. All the samples were packed at the center of the rotor with 3 mm thickness along the axis direction to ensure homogeneity of the r.f. field and temperature.

For all the experiments, the fluorine π/2 pulse width was set to 2.5 μs and the fluorine spin-lock field was 100 kHz. ^{19}F DP measurements for CD ICs required a short spin locking (up to 1 ms) before data acquisition to suppress the background signal since CD ICs are less sensitive than neat Cl-OVDF due to the lower volume fraction of fluorines. The spin-lattice relaxation times in the laboratory frame for fluorine (T_1^F) were measured by inversion recovery technique. The recovery time was varied from 0.01 to 20 s.

Solution-state ^{19}F NMR experiments were carried out on a JEOL AL400 spectrometer at a ^{19}F Larmor frequency of 376.05 MHz. Each sample was dissolved in DMSO-d_6 (2% w/v) before adding $CFCl_3$ as the internal standard. The fluorine π/4 pulse width was set to 5.7 μs and the observational range was 100 kHz. The ^{19}F NMR spectra were obtained with a repetition time of 5.0 s and scans of 256 times.

2.3. Other analytical methods

Infrared (IR) absorption spectra of the CD ICs and the original β-CD were obtained using an AVATAR320 FT-IR spectrometer (Nicolet) mixed with potassium bromide and pressed into pellets. The spectra were recorded with an accumulation of 32 scans with a resolution of 4 cm^{-1}. Differential scanning calorimetric (DSC) measurements were performed with a SHIMADZU DSC-60 in the temperature range between −50 and 250 °C at a heating rate of 10 °C/min. Nitrogen was used as the purge gas.

3. Results and discussion

3.1. Refinement of Cl-OVDF using β-CD

The as-received Cl-OVDF was supposed to be contaminated by impurities such as a catalyst or by-products, which seems to affect not only the crystallization of Cl-OVDF but also the formation of IC with β-CD. Thereby, we carefully prepared samples according to the flow chart shown in Scheme 1 to remove the impurities. When a 'crude IC' was prepared from as-received Cl-OVDF and β-CD in the same way as above, a large amount of Cl-OVDF that had not been incorporated in β-CD remained in a filter drain. Addition of much amount of water to the drain before evaporating organic solvents yielded a mixture of Cl-OVDF and a small amount of β-CD. After complete evaporation of water, Cl-OVDF was extracted by re-dissolving the mixture into acetone and THF. Slow evaporation of the organic solvents allowed Cl-OVDF to recrystallize from solution, resulting in a loose and non-sticky powder. We hereafter refer to the recrystallized Cl-OVDF as 'refined Cl-OVDF'.

Fig. 1 shows the solution-state ^{19}F NMR spectra of (a) as-received and (b) refined Cl-OVDF in DMSO-d_6 (2% w/v) measured at 40 °C. The spectra (c) and (d) demonstrate longitudinally magnified spectra of (a) and (b), respectively. The signal assignments of peaks A–K denoted in the figure are summarized in Table 1 [11,36]. The spectra were normalized by the peak intensity of peak A. Comparing the spectrum (c) with (d), the former shows two signals

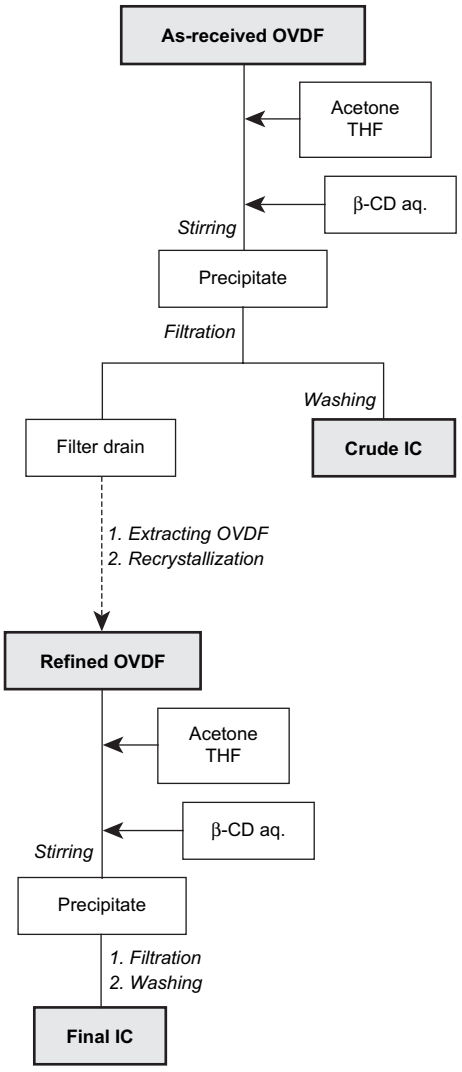

Scheme 1. Flow chart for refinement of Cl-OVDF and preparation of Cl-OVDF/β-CD IC.

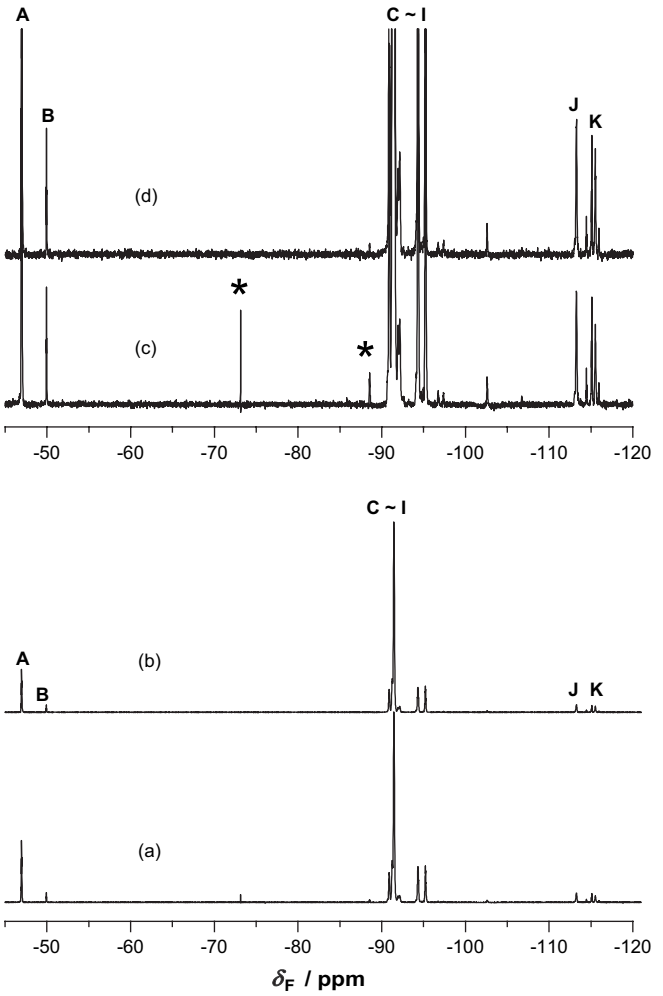

Fig. 1. Solution-state ^{19}F NMR spectra for (a) as-received and (b) refined Cl-OVDF dissolved in DMSO-d_6. The spectra (c) and (d) are longitudinal expansions of (a) and (b), respectively.

at −73.1 and −88.6 ppm (denoted by asterisks), but these are hardly to find in the latter. Since the signals are resonated at different positions from peaks A–K, they can be ascribed to fluorine-containing contaminants having different chemical structures from Cl-OVDF. This also indicates that the contaminants are preferentially incorporated in β-CD than the major component of Cl-OVDF. The contaminants might be by-products generated from catalyst and VDF monomer.

In Fig. 2, the identical spectra with Fig. 1 are depicted on expanded scales: the lower is the as-received Cl-OVDF, while the upper is the refined. It is evident from the figure that each signal except for peak E for the former matches well with that for the latter when they are normalized by peak A. However, peak E of the latter is more intense than that of the former. As shown in Table 1, peak E was assigned to the fluorines at the center of four consecutive repeating units linked in a *head-to-tail* manner (–CH_2CF_2–CH_2CF_2–CH_2CF_2–CH_2CF_2–). Accordingly, the more intense peak E indicates an increase in the proportion of longer chains in the refined Cl-OVDF. Furthermore, this suggests that the shorter chains or LW components are preferentially incorporated in β-CD than the longer chains. In fact, it has been reported that CDs are more likely to include smaller molecules than larger [22], which is also the case for Cl-OVDF.

Fig. 3 shows the DSC curves of (a) as-received and (b) refined Cl-OVDF. A tail of endothermic peak appears near room temperature for (a). Moreover, endothermic peaks are observed for (b) at higher temperature than those in (a). These features agree well with an expectation that the refined Cl-OVDF was obtained by removing LW components and contaminants from as-received Cl-OVDF. However, the DSC curve of (b) also shows several endothermic peaks, indicating that β-CD does not necessarily extract some specific molecular-weight components of Cl-OVDF.

Table 1
^{19}F signal assignments of Cl-OVDF

	δ_F/ppm	Chemical structure	Site in the chain
A	−47.0	–1–1–**1**–Cl	End
B	−49.9	–1–2–**1**–Cl	End
C	−90.9	–**1**–1–1–2–	Regular
D	−91.3	–2–1–1–**1**–	Regular
E	−91.5	–1–**1**–1–1–	Regular
F	−91.9	–1–2–1–**1**–	Regular
G	−92.1	–**1**–1–2–	Regular
H	−94.3	–1–**1**–1–Cl	Near end
I	−95.2	CCl_3–**1**–1–1–	Near end
J	−113.2	–1–**1**–2–1–	Regio-irregular
K	−115.5	–2–**1**–2–2–	Regio-irregular

The numbers 1: CH_2CF_2, 2: CF_2CH_2.

3.2. Molecular structure of refined Cl-OVDF

Fig. 4 shows the FT-IR spectra of (a) as-received and (b) refined Cl-OVDF in the region from 450 to 1550 cm^{-1}. It has been reported

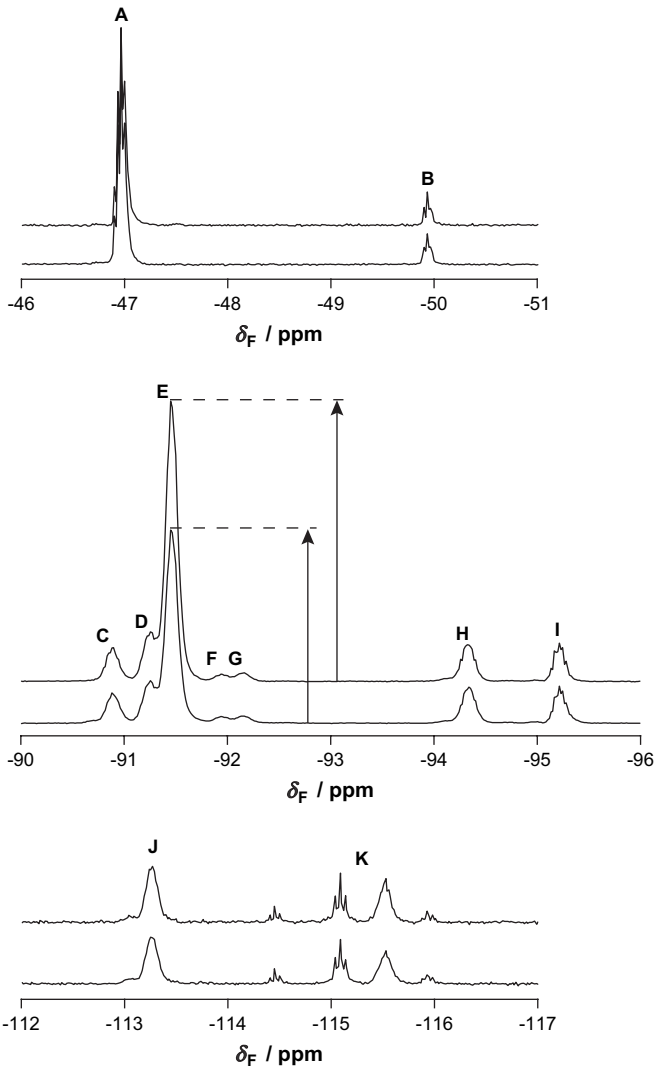

Fig. 2. Solution-state ^{19}F NMR spectra of as-received (lower) and refined Cl-OVDF (upper) on expanded scales of Fig. 1. The horizontal lines and arrows demonstrate the signal intensities for peak E.

that the crystallites of as-received Cl-OVDF are mainly composed of β- or γ-form, and the LW components are likely to take β-form [11,12]. In fact, the spectrum (a) shows characteristic bands for β-form at 511, 840, 1162, 1278 cm^{-1} in addition to those for γ-form at

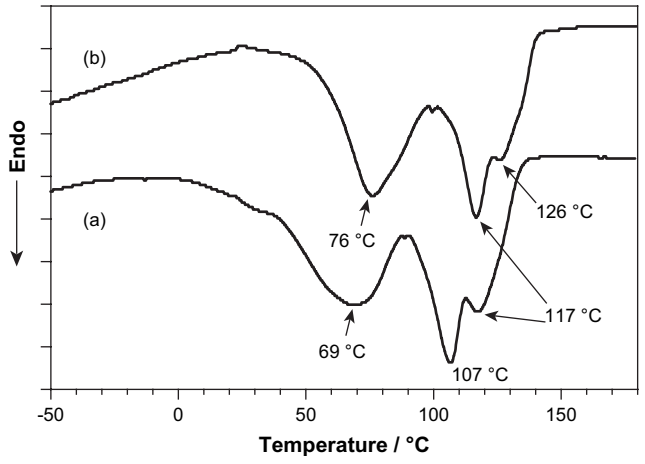

Fig. 3. DSC curves of (a) as-received and (b) refined Cl-OVDF.

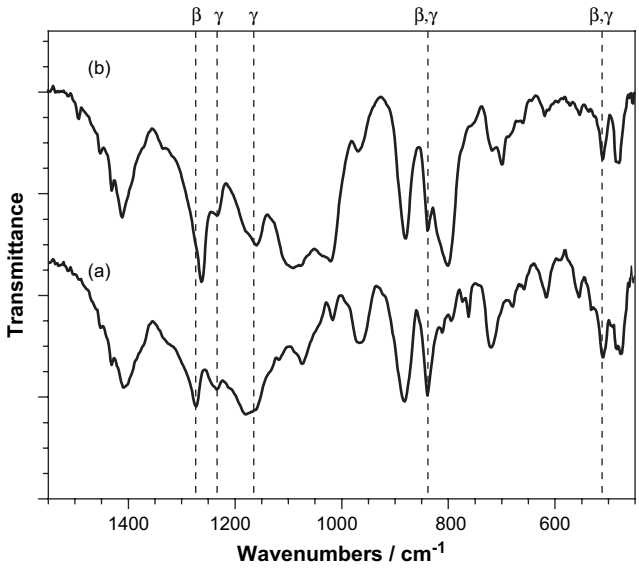

Fig. 4. IR spectra of (a) as-received and (b) refined Cl-OVDF.

511, 835, 1236 cm^{-1} [1–10]. Although additional intense bands are observed in the region from 700 to 1200 cm^{-1}, the characteristic bands for β- and γ-form are still recognizable in the spectrum (b). This indicates that the refined Cl-OVDF takes both β- and γ-form as well as the as-received Cl-OVDF.

Fig. 5 shows the solid-state $^1H \rightarrow {}^{19}F$ CP/MAS NMR spectra of (a) as-received and (b) refined Cl-OVDF measured at 40 °C (depicted by thick solid lines). The contact time for CP was set to 0.1 ms. It is well known that the polymorphs of PVDF crystallites (α-, β-, and γ-form) are readily distinguishable by the line shapes of the crystalline components observed in ^{19}F MAS spectra [33,37]. The difference in the line shapes becomes more distinct when the fluorines in the immobile crystallites are selectively observed using the $^1H \rightarrow {}^{19}F$ CP technique. In the case of Cl-OVDF, $^1H \rightarrow {}^{19}F$ CP/MAS spectra are more preferable to identify the morphologies in crystalline domains than ^{19}F direct polarization (DP) MAS spectra because the amorphous signals are too intense at ambient temperature. The spectrum (a) can be well fitted by four Lorentzian functions located at −85, −91, −94, and −101 ppm (depicted by thin solid lines). They are denoted as peaks 2–5 in turn, and the summation of the peaks is shown by a dotted line. This indicates that Cl-OVDF chains in the as-received crystallites take γ-form, in which the fluorines are resonated at four different chemical shifts. Note that peak 4 is much more intense than the other peaks. Because pure γ-form crystallites would give four equi-intense peaks, the larger intensity of peak 4 indicates that a significant amount of β-form crystallites resonated at −94 ppm [37] is incorporated. The spectrum (b) can also be fitted by the four Lorentzian functions at the same chemical shifts as spectrum (a). However, unlike the spectrum (a), the intensity of peak 4 is close to those of the other peaks, which clearly indicates that γ-form is predominant in the refined Cl-OVDF. As mentioned above, the LW components are likely to take β-form, while the higher-molecular-weight (HW) components are composed of β- and γ-form [11,12]. Accordingly, the weaker signal of peak 4 in the refined Cl-OVDF can be explained in terms that the LW components were effectively excluded from the crude Cl-OVDF by the IC formation.

Fig. 6 shows the variable-temperature (VT) ^{19}F DP spectra of refined Cl-OVDF at the temperature range between 0 and 80 °C. The spinning sidebands (SSBs) derived from peaks 2 to 5 are also shown in the figure. Note that the signal at −47 ppm (peak 1) indicated by arrows is assignable to the fluorines at the end group (–CF_2Cl) in the

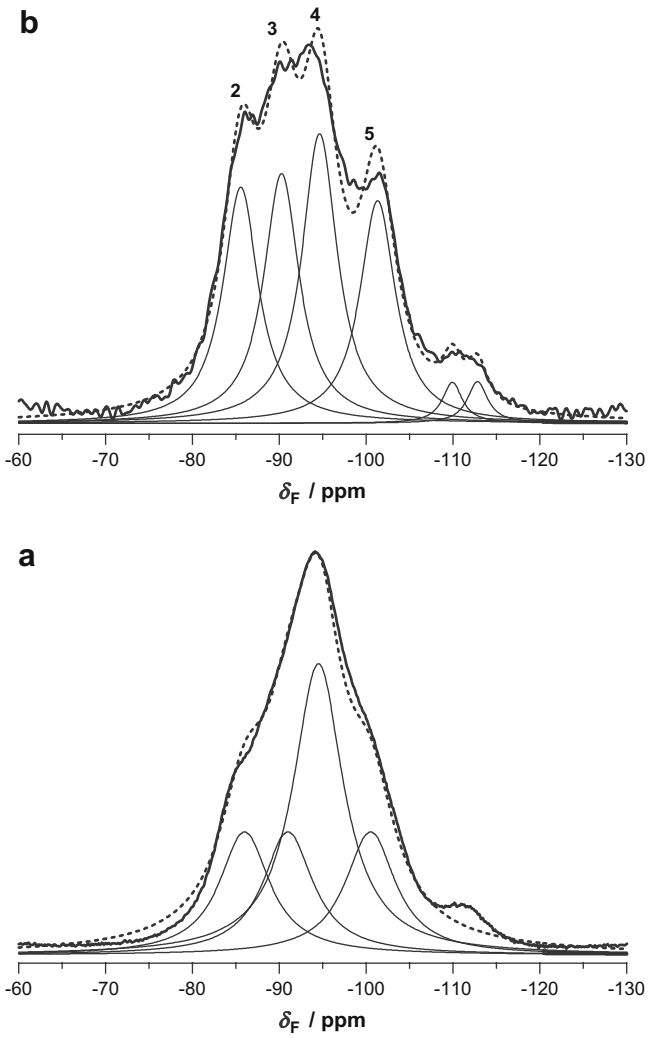

Fig. 5. Solid-state $^1H \rightarrow {}^{19}F$ CP/MAS NMR spectra of (a) as-received and (b) refined Cl-OVDF obtained at 40 °C. The contact time used was 0.1 ms.

crystallites. Comparing the SSBs with the corresponding central signals, peak 1 is recognizable though it is overlapped with the SSB of peak 5. Above 40 °C, sharp signals attributable to the amorphous or rubbery state become intense due to the onset of fusion as suggested by the DSC measurements. At 80 °C, only the amorphous signals look recognizable, but this is just a result of normalization by the maximum signal level. On the contrary, the VT $^1H \rightarrow {}^{19}F$ CP/MAS spectra shown in Fig. 7 clearly demonstrate that the crystalline signals are certainly observed up to 80 °C. However, the signal-to-noise (S/N) ratio of the CP/MAS spectra deteriorates as the temperature increases because of the vigorous motions of Cl-OVDF chains that accompany partial melting of crystallites.

3.3. Structure and dynamics of Cl-OVDF/β-CD inclusion compound

A well-defined Cl-OVDF/β-CD IC was prepared from the refined Cl-OVDF (0.085 g) and β-CD aqueous solution (30 ml) in the same way as described above. To confirm the formation of IC, we performed an additional DSC measurement for Cl-OVDF/β-CD IC and the obtained curve is drawn in Fig. 8(a). Since the first heating curve exhibits a huge endothermic peak due to the vaporization of crystal water, the curve in the figure was obtained in the second heating scan. For comparison, the DSC curves of $C_{20}F_{42}$/β-CD and pure β-CD, which have been reported in a previous study [28], are also shown as (b) and (c). Compared with Fig. 3, the curve for Cl-OVDF/β-CD IC

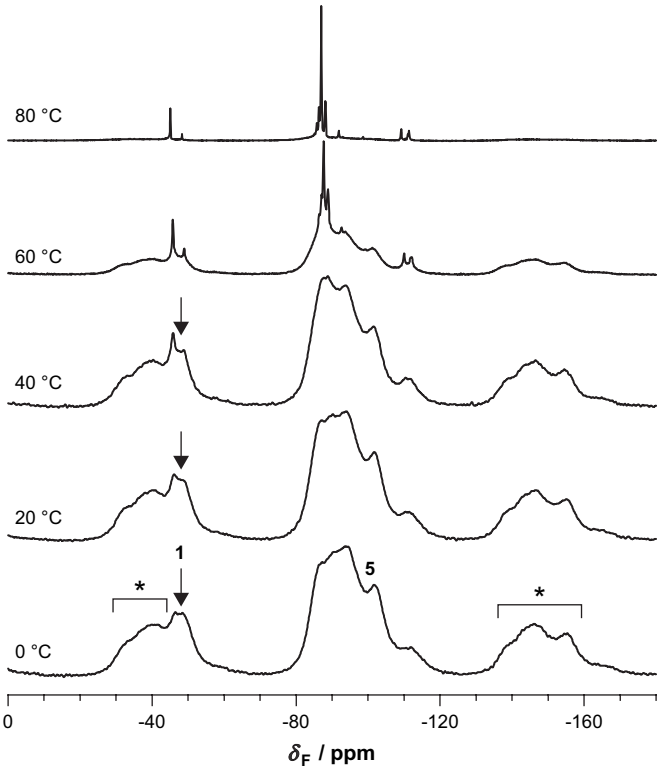

Fig. 6. Variable-temperature (VT) ^{19}F DP MAS NMR spectra of refined Cl-OVDF. Spinning sidebands are denoted by asterisks.

does not show any endothermic peak derived from neat Cl-OVDF, but shows a weak exothermic peak at ca. 35 °C. As it is evident from Fig. 8, such an exothermic peak is not observed for pure β-CD, but is also observed for $C_{20}F_{42}$/β-CD IC. In the previous study [28], we

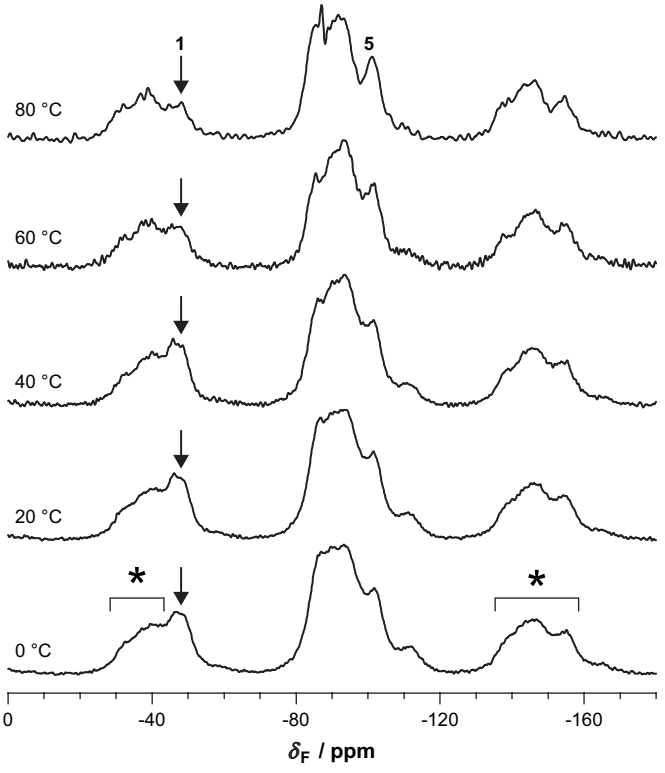

Fig. 7. VT $^1H \rightarrow {}^{19}F$ CP/MAS NMR spectra of refined Cl-OVDF. The contact time used was 0.2 ms. Spinning sidebands are denoted by asterisks.

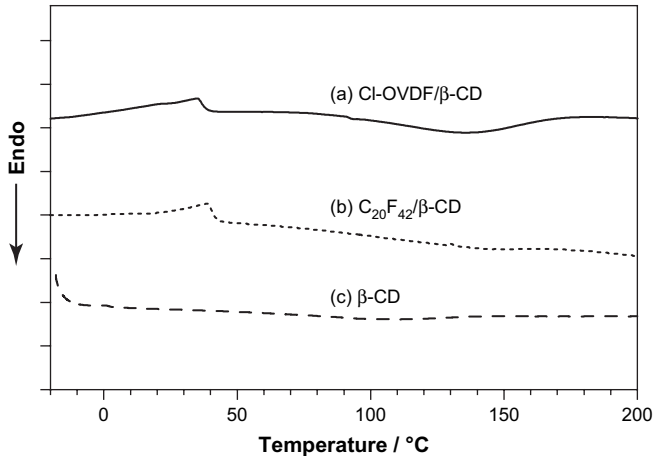

Fig. 8. (a) DSC curve of Cl-OVDF/β-CD IC. For comparison, the curves of (b) *n*-$C_{20}F_{42}$/β-CD IC and (c) pure β-CD are also shown [28].

pointed out that the exothermic peak could be associated with a certain type of crystallization leading to form ordered channel-type structures. Therefore, we consider that Cl-OVDF/β-CD IC might have similar structure to $C_{20}F_{42}$/β-CD IC.

Fig. 9 shows the ^{19}F DP spectra of (a) refined Cl-OVDF and (b) Cl-OVDF/β-CD IC measured at 60 °C. The spectrum (a) is identical with that in Fig. 6. Here, we refer to 'refined Cl-OVDF' as 'neat Cl-OVDF' for comparison with the IC. As it is evident from the figure, the ^{19}F chemical shifts of IC are closer to those of the amorphous signals rather than the γ-crystalline signals observed for neat Cl-OVDF. This can be explained in two ways: (1) the Cl-OVDF main chains in the IC undergo faster conformational changes than the timescale of NMR observation or (2) the main chains happen to take an unknown conformation different from α-, β-, and γ-form. Fig. 10 shows the VT ^{19}F DP spectra of Cl-OVDF/β-CD IC measured at −40 to

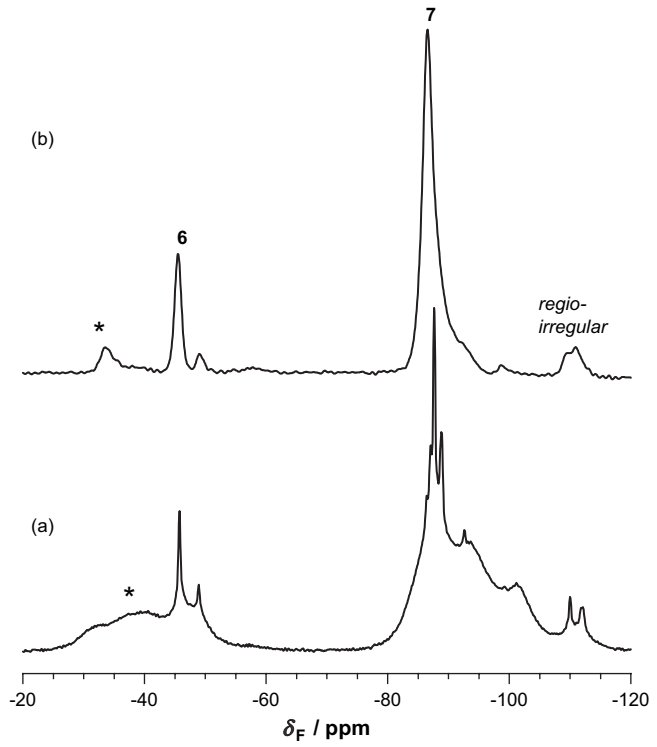

Fig. 9. ^{19}F DP MAS spectra of (a) refined Cl-OVDF and (b) Cl-OVDF/β-CD IC measured at 60 °C. ^{19}F signal assignments are also shown. Spinning sidebands are denoted by asterisks.

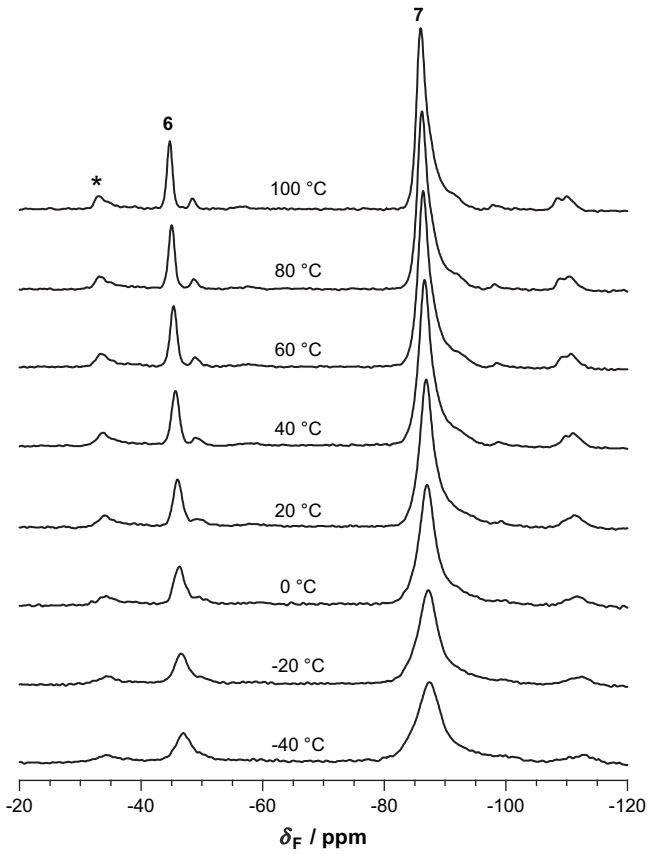

Fig. 10. VT ^{19}F DP MAS NMR spectra of Cl-OVDF/β-CD.

100 °C. The fluorine signals of $-CF_2Cl$ and $-CH_2CF_2-$ are denoted as peaks 6 and 7, respectively. Both peaks become gradually broadened as the temperature decreases. However, we cannot find any signals assignable to the given crystalline conformations even at −40 °C. In addition, the spectral shapes of the VT ^{1}H → ^{19}F CP/MAS spectra are nearly the same as those of the VT ^{19}F DP spectra (not shown in the figure) when they are compared at each temperature. Hence, the Cl-OVDF chains incorporated in β-CD channel do not converge to any specific conformations but become more widely distributed as the temperature decreases. For more exact discussions about the molecular mobility, we observed the temperature dependence of the magnetic relaxation parameters as follows: the spin-lattice relaxation time in the laboratory frame (T_1^F) and that in the rotating frame ($T_{1\rho}^F$). In general, the former is sensitive to the molecular motions near the Larmor frequency (ca. 376 MHz), while the latter is strongly affected by the molecular motions of which the frequencies are close to the spin-lock frequency (ca. 100 kHz).

Fig. 11 shows the variation of T_1^F as a function of temperature, in which the T_1^F values for neat Cl-OVDF and Cl-OVDF/β-CD IC are plotted by filled and open symbols, respectively. Since peaks 2–4 take almost identical values with peak 5, only the T_1^F values for peaks 1, 5–7 are shown for clarity. Note that neat Cl-OVDF gives amorphous signals at 40 °C and above (Fig. 6). A comparison of the T_1^F values for the amorphous signals of neat Cl-OVDF and those for Cl-OVDF/β-CD IC is summarized in Table 2. The T_1^F values of crystalline Cl-OVDF are slightly decreased as the temperature increases (Fig. 11). The fact that the T_1^F for peak 1 is almost identical to that for peak 5 is owing to the overlap of SSB as mentioned above. Meanwhile, the T_1^F of amorphous Cl-OVDF rapidly drops off and reaches a value below 1 s at 80 °C (Table 2). This indicates that the molecular motions at the frequency of several hundreds of MHz substantially exist in the amorphous domains at that temperature. It is

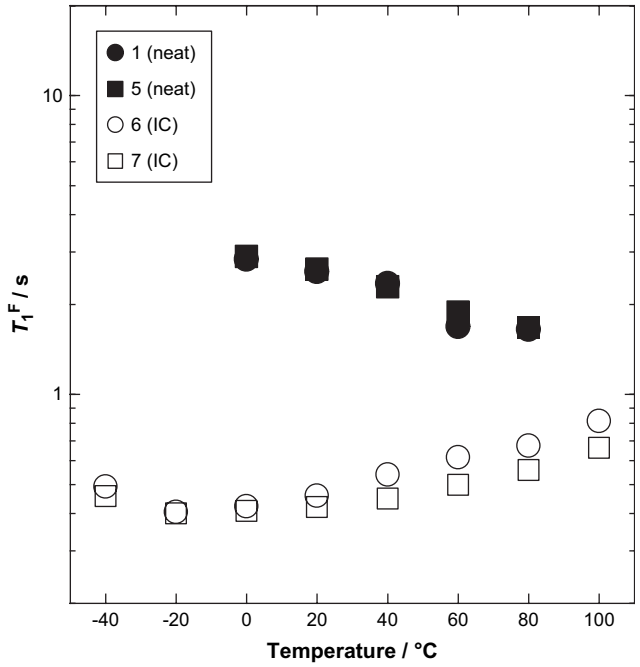

Fig. 11. Temperature dependence of T_1^F values for $-CF_2Cl$ and $-CH_2CF_2-$ signals for neat Cl-OVDF (filled symbols) and Cl-OVDF/β-CD IC (open symbols).

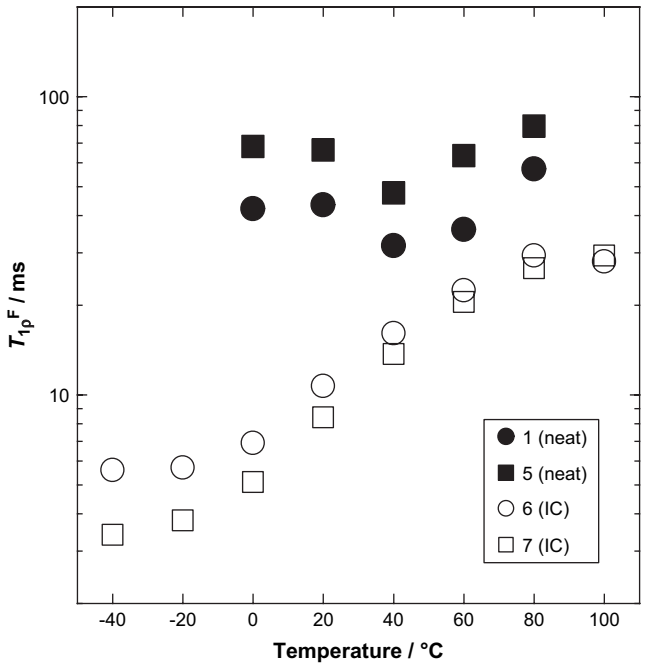

Fig. 12. Temperature dependence of $T_{1\rho}^F$ values for $-CF_2Cl$ and $-CH_2CF_2-$ signals for neat Cl-OVDF (filled symbols) and Cl-OVDF/β-CD IC (open symbols).

Table 2
T_1^F values of CF_2Cl and CH_2CF_2 fluorines in amorphous Cl-OVDF and those in Cl-OVDF/β-CD IC (unit: s)

	CF_2Cl		CH_2CF_2	
	Amorphous	IC	Amorphous	IC
40 °C	2.1	0.54	2.2	0.45
60 °C	1.4	0.62	1.5	0.50
80 °C	0.82	0.67	0.61	0.56

likely that the internal rotation of $-CF_2Cl$ at the termini and the librations of C–C bonds are responsible for such motions [26,28]. The T_1^F of amorphous Cl-OVDF was expected to take a minimum above 80 °C, although the measurements were not performed at higher temperatures because the sample possibly runs out of a spinning rotor. In contrast, the T_1^F values of Cl-OVDF/β-CD IC are consistently smaller than those of the crystalline Cl-OVDF in the temperature range of NMR measurements. In addition, the T_1^Fs of IC are comparable with those of the amorphous Cl-OVDF at 80 °C (Table 2). These results agree with the fact that the ^{19}F chemical shifts of IC are close to those of the amorphous Cl-OVDF (Fig. 9), which supports that the Cl-OVDF chains incorporated in IC undergo faster molecular motions than the NMR timescale. The T_1^F of peak 6 reaches a minimum at −20 °C, indicating that the frequency of the internal rotation of $-CF_2Cl$ approaches the Larmor frequency at that temperature. It should be pointed out that the temperature range of the T_1^F minimum for the IC is lower by approximately 100 K than that for the amorphous Cl-OVDF, although the T_1^F minimum was not clearly observed for the neat Cl-OVDF above 80 °C. This indicates that the internal rotation at the end group can be more vigorous in the IC cavities than the amorphous phase in the bulk. The T_1^F of peak 7 also reaches a minimum at −20 °C, which is mainly caused by the librations of C–C bonds. Moreover, the intramolecular spin diffusion from the fluorine nuclei at $-CF_2Cl$ to $-CH_2CF_2-$ may also occur in the lower temperature range where the T_1^Fs of peaks 6 and 7 agree well [28].

Fig. 12 shows the variation of $T_{1\rho}^F$ as a function of temperature. The symbols in the figure are identical with those in Fig. 11. A comparison of the $T_{1\rho}^F$ values for the amorphous Cl-OVDF and those for Cl-OVDF/β-CD IC is summarized in Table 3. The $T_{1\rho}^F$ values of the crystalline Cl-OVDF are larger than 30 ms in the temperature range of measurements, which is an indicative of the lack of motions around the spin-lock frequency (100 kHz) in the crystallites. In contrast, the $T_{1\rho}^F$ values of Cl-OVDF/β-CD IC are smaller than those of the crystalline Cl-OVDF at every temperature, which is in common with the temperature dependence of the T_1^F values. The $T_{1\rho}^F$s of Cl-OVDF/β-CD IC seem to take a minimum at ca. −40 °C, although we cannot measure the spectra below −40 °C due to the lower temperature limit of probe apparatus. As shown in Fig. 11, the temperature dependences of T_1^F values for peaks 6 and 7 are almost identical, in particular near the minimum region, while those of $T_{1\rho}^F$ values differ by several ms (Fig. 12). Hence, the Cl-OVDF chains in the IC are unlikely to undergo a uniform and uniaxial motion because it should give an identical $T_{1\rho}^F$ value [38]. In other words, the plausible motion that affects the $T_{1\rho}^F$ values in the IC is more similar to the motion in the amorphous phase rather than that in the rotator phase which has been discussed for *n*-alkanes. In fact, as shown in Table 3, the $T_{1\rho}^F$ values of $-CF_2Cl$ fluorines are comparable with those of $-CH_2CF_2-$ fluorines in the IC. However, the $T_{1\rho}^F$s of these fluorines in the amorphous Cl-OVDF are clearly different at 80 °C ($-CF_2Cl$, 83 ms; $-CH_2CF_2-$, 35 ms). This indicates that more significant ^{19}F spin diffusion occurs in the IC than in the amorphous phase of the bulk. We consider that this is an essential difference between the amorphous Cl-OVDF and Cl-OVDF/β-CD, which may be due to the fact that the Cl-OVDF chains in the amorphous bulk can move in the three-dimensional space, while only one-dimensional translational motion is allowed for the Cl-OVDF chains confined in IC cavities.

Table 3
$T_{1\rho}^F$ values of CF_2Cl and CH_2CF_2 fluorines in amorphous Cl-OVDF and those in Cl-OVDF/β-CD IC (unit: ms)

	CF_2Cl		CH_2CF_2	
	Amorphous	IC	Amorphous	IC
40 °C	18	16	13	14
60 °C	16	22	14	21
80 °C	83	29	35	25

4. Conclusions

The molecular structure and dynamics of a vinylidene fluoride oligomer telomerized by carbon tetrachloride (Cl-OVDF) have been investigated using solid-state ^{19}F MAS NMR spectroscopy. Cl-OVDF chains in as-received crystallites are likely to take both β- and γ-form conformations. However, Cl-OVDF was refined by the preferential formation of β-CD ICs with contaminants and lower-molecular-weight (LW) components. As a result, the remaining higher-molecular-weight (HW) components form nearly pure γ-form crystallites. The refined Cl-OVDF successfully forms an IC with β-CD (Cl-OVDF/β-CD IC). Inside the β-CD cavities, virtually isolated Cl-OVDF chains do not take any specific conformation even at −40 °C despite the broadened distribution in the main chain structures. In other words, the neighboring molecules play an important role in the crystallization process of Cl-OVDF rather than the energetic stability of isolated chains. The IC formation of oligomers and polymers with β-CDs is a convenient method for investigation of the structure and dynamics of virtually isolated chains.

Acknowledgement

We thank Prof. Norimasa Okui for the discussions on the crystal polymorphs and physical properties of OVDF and PVDF.

References

[1] Gregorio Jr R, Cestari M. J Polym Sci Part B 1994;32:859–70.
[2] Prest Jr WM, Luca DJ. J Appl Phys 1978;49:5042–7.
[3] Salimi A, Yousefi AA. J Polym Sci Part B 2004;42:3487–95.
[4] Tashiro K, Hanesaka M. Macromolecules 2002;35:714–21.
[5] Peng Y, Wu P. Polymer 2004;45:5295–9.
[6] Kobayashi M, Tashiro K, Tadokoro H. Macromolecules 1975;8:158–71.
[7] Bachmann MA, Gordon WL, Koenig JK, Lando JB. J Appl Phys 1979;50:6106–12.
[8] Tashiro K, Kobayashi K, Tadokoro H. Macromolecules 1981;14:1757–64.
[9] Benedetti E, D'Alessio A, Bertolutti C, Vergamini P, Fanti ND, Pianca M, et al. Polym Bull 1989;22:645–51.
[10] Park J, Seo Y, Kim I, Ha C, Aimi K, Ando S. Macromolecules 2004;37:429–36.
[11] Herman Uno T, Kubono A, Umemoto S, Kikutani T, Okui N. Polymer 1997;38:1677–83.
[12] Herman, Umemoto S, Kikutani T, Okui N. Polym J 1998;30:659–63.
[13] Yoshida Y, Ishida K, Ishizaki K, Horiuchi T, Matsushige K. Jpn J Appl Phys 1997;36:7389.
[14] Noda K, Ishida K, Kubono A, Horiuchi T, Yamada H, Matsushige K. Jpn J Appl Phys 2000;39:6358–63.
[15] Noda K, Ishida K, Kubono A, Horiuchi T, Yamada H, Matsushige K. Jpn J Appl Phys 2001;40:4361–4.
[16] Szejtli J. Chem Rev 1998;98:1743–53.
[17] Schneider H, Hacket F, Rüdiger V, Ikeda H. Chem Rev 1998;98:1755–85.
[18] Harata K. Chem Rev 1998;98:1803–27.
[19] Nepogodiev SA, Stoddart JF. Chem Rev 1998;98:1959–76.
[20] Harada A. Carbohydr Polym 1997;34:183–8.
[21] Harada A, Li J, Kamachi M. Macromolecules 1994;27:4538–43.
[22] Harada A, Li J, Suzuki S, Kamachi M. Macromolecules 1993;26:5267–8.
[23] Girardeau TE, Leisen J, Beckham HW. Macromol Chem Phys 2005;206:998–1005.
[24] Lu J, Mirau PA, Tonelli AE. Macromolecules 2001;34:3276–84.
[25] Lu J, Mirau PA, Daniel Shin I, Nojima S, Tonelli AE. Macromol Chem Phys 2002;203:71–9.
[26] Lu J, Mirau PA, Tonelli AE. Prog Polym Sci 2002;27:357–401.
[27] Saalwächter K. Macromol Rapid Commun 2002;23:286–91.
[28] Tatsuno H, Ando S. J Phys Chem B 2006;110:25751–60.
[29] Jiao H, Goh SH, Valiyaveettil S, Zheng J. Macromolecules 2003;36:4241–3.
[30] Nostro PL, Santoni I, Bonini M, Baglioni P. Langmuir 2003;19:2313–7.
[31] Druliner JD, Wasserman E. J Fluorine Chem 1995;72:75–8.
[32] Ando S, Harris RK, Scheler U. Supplement of encyclopedia nuclear magnetic resonance. Chichester: John Wiley & Sons; 2000 [chapter 9].
[33] Holstein P, Scheler U, Harris RK. Polymer 1998;39:4937–41.
[34] Holstein P, Monti GA, Harris RK. Phys Chem Chem Phys 1999;1:3549–55.
[35] Ando S, Harris RK, Reinsberg SA. Magn Reson Chem 2002;40:97–106.
[36] Wormald P, Apperley DC, Beaume F, Harris RK. Polymer 2003;44:643–51.
[37] Hucher C, Beaume F, Eustache RP, Tekely P. Macromolecules 2005;38:1789–96.
[38] Aimi K, Ando S. Magn Reson Chem 2004;42:577–88.
[39] Aimi K, Ando S, Avalle P, Harris RK. Polymer 2004;45:2281–90.
[40] Ando S, Harris RK, Hazendonk P, Wormald P. Macromol Rapid Commun 2005;26:345–56.
[41] Brouwer EB, Challoner R, Harris RK. Solid State Nucl Magn Reson 2000;18:37–52.
[42] Aliev AE, Harris KDM. Magn Reson Chem 1994;32:366–9.